CRISPRi-based functional genomic screening identifies genes essential for CH_4-dependent growth in the methanotroph *Methylococcus capsulatus* Bath.

Jessica M. Henard, Spencer A. Lee, Yao-Chuan Yu, Danyang Shao, Rajeev K. Azad, and Calvin A. Henard*.

Department of Biological Sciences and BioDiscovery Institute, University of North Texas, Denton, TX, USA.

*Correspondence to Calvin.Henard@unt.edu

Running title: Methanotroph CRISPRi

Keywords: methanotroph, CRISPRi, methane monooxygenase, RubisCO, functional genomics

Abstract

Aerobic methanotrophic bacteria are the primary organisms that consume atmospheric methane (CH_4) and have potential to mitigate the climate-active gas. However, a limited understanding of the genetic determinants of methanotrophy hinders the development of biotechnologies leveraging these unique microbes. Here, we developed and optimized a methanotroph CRISPR interference (CRISPRi) system to enable functional genomic screening. We built a genome-wide single guide RNA (sgRNA) library in the industrial methanotroph, *Methylococcus capsulatus*, consisting of ~45,000 unique sgRNAs mediating inducible, CRISPRi-dependent transcriptional repression. A selective screen during growth on CH_4 identified 233 genes whose transcription repression resulted in a fitness defect and repression of 13 genes associated with a fitness advantage. Enrichment analysis of the 233 putative essential genes linked many of the encoded proteins with critical cellular processes like ribosome biosynthesis, translation, transcription, and other central biosynthetic metabolism, highlighting the utility of CRISPRi for functional genetic screening in methanotrophs, including the identification of novel essential genes. *M. capsulatus* growth was inhibited when the CRISPRi system was used to individually target genes identified in the screen, validating their essentiality for methanotrophic growth. Collectively, our results show that the CRISPRi system and sgRNA library developed here can be used for facile gene-function analyses and genomic screening to identify novel genetic determinants of methanotrophy. These CRISPRi screening methodologies can also be applied to high-throughput engineering approaches for isolation of improved methanotroph biocatalysts.

Introduction

Aerobic methanotrophic bacteria, methanotrophs, play an essential role in balancing atmospheric carbon by oxidizing methane (CH_4) to multi-carbon molecules (methanotroph biomass) and carbon dioxide (CO_2). These ubiquitous microbes limit the escape of CH_4 to the atmosphere via biofiltration in terrestrial and aquatic systems[1]. Methanotrophs can also be leveraged for the bioconversion of abundant CH_4-rich gas streams from oil and natural gas extraction sites, coal mines, agricultural waste, landfills, and wastewater treatment facilities, and have the potential to capture rising CH_4 greenhouse gas and mitigate climate change[2]. However, significant advances in methanotroph biology and engineering for effective CH_4 capture and conversion are needed to realize cost-effective solutions using methanotrophs.

Methanotrophs belong to a broad group of methylotrophic microbes that use organic single carbon (C_1) molecules as sources of carbon and/or energy, which, in addition to CH_4, includes methanol (CH_3OH), formate (CH_2O), and/or methylamine. Unique to methanotrophs is the CH_4 monooxygenase (MMO) enzyme that oxidizes the strong C-H bond of CH_4 to generate CH_3OH[3]. Methanotroph C_1 metabolic enzymes and pathways for CH_3OH assimilation to biomass and its dissimilation to CO_2 generally overlap with those in methylotrophs[4]. These include the ribulose monophosphate and serine cycles used by Gammaproteobacterial methanotrophs and Alphaproteobacterial methanotrophs for C_1 assimilation, respectively[5–7]. In addition, the methanotroph dissimilatory metabolic processes that couple C_1 oxidation to the electron transport chain for ATP production are coincident with those in other methylotrophs[89]. The central CH_4 metabolic pathways have been biochemically validated using radiolabeled isotopes in a subset of methanotrophs[5,7,10]. Additionally, the availability of several complete methanotroph genomes and comparative genomics have provided critical insight into methanotroph CH_4 metabolism[11–18]. However, many genes that may be required for methanotrophy, especially those outside of the core C_1 metabolic gene clusters, are unknown.

Early research using chemical and insertional transposon mutagenesis of the CH_3OH-utilizing methylotrophic bacterium *Methylobacterium extorquens* AM1 identified many genes required for methylotrophic growth, including those encoding the enzymes needed for methanol oxidation, formaldehyde oxidation, formate oxidation, and assimilation via the serine cycle[19–23624–26]. Additionally, transposon mutagenesis led to the identification of genes required for transport and utilization of rare earth elements[27] and transcriptional regulators of the C_1 metabolic pathways[20,28]. Notably, the elucidation of genes required for methylotrophy was enabled by leveraging their facultative capacity to utilize alternative multi-carbon sources (i.e. succinate) supplied during library generation[28]. In contrast, the vast majority of methanotrophs are obligate CH_4-utilizers; thus, mutations in essential genes required for growth on CH_4 would be lost from the mutagenized population. However, there are only two reports of successful chemical mutagenesis[29] and one report of transposon insertional mutagenesis[30] in methanotrophs,

underscoring barriers applying forward genetic techniques to CH_4-oxidizing bacteria and significant knowledge gaps related thereto.

Clustered regularly interspaced short palindromic repeats (CRISPR) interference (CRISPRi) is a genetic tool that has been leveraged for functional genetic screens in diverse bacteria[31–39]. CRISPRi uses the nuclease-deficient CRISPR-associated (Cas) variant dCas9 and a single-guide RNA (sgRNA) for the sequence-specific repression of gene expression[40]. This technology can be used to target single genes or scaled for genome-wide screening via massively parallel oligonucleotide synthesis of pooled sgRNAs. Functional genomic screens using CRISPRi are coupled with next generation sequencing to quantify the depletion or enrichment of sgRNAs (sgRNA differential fitness) during selective bacterial cultivation[41]. Notably, transcription repression by CRISPRi can be tightly regulated using inducible promoters to drive dCas9 and/or sgRNA expression; thus, in contrast to transposon mutagenesis, CRISPRi can be applied to conditionally evaluate the effect of repressing essential gene expression on bacterial growth. Recent developments of methanotroph CRISPR genome editing tools indicate that Cas9 and sgRNAs are functional in Gammaproteobacterial and Alphaproteobacterial methanotrophs[31,42–46] paving the way for CRISPRi and forward genetic approaches in methanotrophs that have eluded these bacteria for decades.

Here, we modified a previously developed methanotroph CRISPR-Cas9 genome editing system[44] to facilitate CRISPRi and demonstrate its utility for repressing gene transcription in the phylogenetically diverse methanotrophs *Methylococcus capsulatus* Bath and *Methylosinus trichosporium* OB3b. We performed a genome-scale CRISPRi screen using 45,798 unique sgRNAs targeting all annotated genes in the *M. capsulatus* Bath genome to investigate gene-function relationships during CH_4 cultivation. We identified 429 genes whose transcription repression resulted in significantly decreased fitness and repression of 5 genes associated with a fitness advantage. sgRNAs with decreased fitness scores targeted genes encoding proteins involved in critical cellular processes like ribosome biosynthesis, translation, transcription, and central biosynthetic metabolism, underscoring the utility of CRISPRi for the identification of predicted and novel essential genes. The screen provides genetic evidence that the Entner-Doudoroff pathway is essential for CH_4 assimilation and the tetrahydromethanopterin pathway is the primary route for CH_4 dissimilation in *M. capsulatus*. Additionally, the decreased fitness of sgRNAs targeting the ribulose bisphosphate carboxylase/oxygenase (RubisCO) and RubisCO activase genes reiterate the essentiality of CO_2 assimilation for *M. capsulatus* growth on CH_4. The CRISPRi system and sgRNA library developed here can be used for facile gene-function analyses and genomic screening to identify methanotroph genetic determinants under an array of screening conditions. Further, these CRISPRi screening methodologies can also be applied to high-throughput engineering approaches for isolation of improved methanotroph biocatalysts.

Materials and Methods

Bacterial strains and cultivation. Bacterial strains used in this study are shown in Table 1. *E. coli* strains were cultured in lysogeny broth (Lennox) with 25 µg/mL kanamycin, 50 µg/mL spectinomycin, or 10 µg/mL gentamicin for transformant selection. *Methylococcus capsulatus* Bath and *Methylosinus trichosporium* OB3b frozen stocks were streaked onto nitrate mineral salts (NMS) solid medium and maintained in stainless steel gas chambers supplied with 20% CH_4 in the gas phase at 37°C or 30°C, respectively, as previously described[44]. Methanotroph strains were passaged weekly for 4 weeks (maximum passage = 5) after which time a new culture from frozen stock was initiated. Plasmids were transferred to methanotrophs via biparental mating by spreading equivalent biomass of S17-1λ *E. coli* and recipient methanotroph biomass on NMS mating agar mating plates and incubating in a 20% CH_4 atmosphere for 24 h as previously described [44]. After mating, methanotroph transformants harboring plasmids were selected on NMS medium containing 50 µg/mL spectinomycin (pJHCi and derivatives), 10 µg/mL gentamicin (pDS1), and/or 50 µg/mL kanamycin (pJHint). Methanotrophs were cultured in 150 mL vials containing 10 mL of NMS medium at 37°C (*M. capsulatus*) or 30°C (*M. trichosporium*) at 200 rpm orbital shaking. After inoculation with plate-derived biomass to OD_{600} 0.01, vials were crimped with gray butyl stoppers to create gas-tight seals followed by CH_4 addition to the headspace via syringe to reach a final CH_4 concentration of 20% in air (v/v). Where applicable, sgRNA and/or dCas9 expression were induced with 0.2 µg/mL anhydrotetracycline (aTc).

CRISPRi plasmid construction and sgRNA exchange. Primers and other synthetic DNA used in this study are shown in Table 2. To construct a broad-host-range, single plasmid CRISPRi system, we amplified a P_{mxaF}-sgRNA with an mRFP spacer sequence from the pgRNA plasmid[44] using primers oCAH267/289 and ligated it with pCAH01^{SpR}::Cas9[44] linearized with primers oCAH230/231 via isothermal assembly using HiFi Gibson Assembly Master Mix (New England Biolabs). We then amplified the dCas9 gene from plasmid pdCas9-bacteria[40] with oCAH952/1507 and assembled it with the above plasmid backbone amplified with oCAH4/3, exchanging the Cas9 gene with dCas9 to generate plasmid pJHCi. The aTc-inducible suicide plasmid pJHint was constructed via isothermal assembly of the following six DNA fragments: 1) pUC origin of replication from pCAH01 amplified with oCAH403/404; 2) 1kb upstream homology arm amplified with oCAH405/406 from *M. capsulatus* genomic DNA; 3) P_{tet} promoter/operator amplified from pCAH01 with oCAH407/408 ; 4) *tetR*-kn^R cassette from pCAH01 amplified with oCAH409/410; 5) 1kb downstream homology arm amplified with oCAH411/412 from *M. capsulatus* genomic DNA; and 6) *oriT* origin of transfer amplified from pCAH01 with oCAH413/414. pJHint was then amplified with primers oCAH3/4 and assembled with the dCas9 gene fragment to generate plasmid pJHintdCas9. pJHindCas9 was transferred to *M. capsulatus* Bath via conjugation and transformants with the P_{tet}-dCas9 module integrated into their chromosome were selected on NMS solid medium containing 25 µg/mL kanamycin. Successful integration was confirmed via PCR using primers oCAH447/448 that flank the integration site. For sgRNA expression, we initially amplified the mRFP targeting sgRNA from pJHCi with primers oCAH1083/1081 and cloned it into pCAH01 amplified without a ribosomal binding site with primers oCAH4/119 to generate p01sgRNA^{mrfp}. Other aTc-inducible sgRNA

157 expression plasmids were generated by exchanging the spacer sequence via isothermal assembly
158 of a single-stranded oligo containing a unique spacer and the pCAH01sgRNA^{mrfp} amplified with
159 primers oCAH1190/119.
160
161 ***Fluorescence measurement.*** pJHCi was transferred to *M. capsulatus* Bath or *M. trichosporium*
162 OB3b harboring the pDS1 mRFP reporter plasmid via conjugation. Alternatively, pDS1 and
163 p01sgRNA^{mrfp} were iteratively transferred to the *M. capsulatus* Bath strain with chromosomally
164 integrated P_{tet}-dCas9. Overnight seed cultures of these strains were subcultured to OD_{600} = 0.01
165 in liquid medium containing appropriate antibiotics with or without aTc induction and cultivated
166 for 72h to ~ OD_{600} 2.0. 200 µL culture was transferred to a 96-well microplate, and mRFP1
167 fluorescence (ex_{532nm}, em_{588nm}, gain = 80) and optical density (A_{600nm}) was measured with a
168 BioTek Synergy Mx microplate reader. The data were normalized by dividing raw fluorescence
169 reads by the optical density.
170
171 ***Construction of pLSQ and cbbL PAM mutant.*** The *M. capsulatus* Bath *cbbLSQ* operon
172 (MCA2743-2746) including 150bp upstream of *cbbL* presumed to contain the *cbbL* promoter
173 was amplified from purified genomic DNA using primers oCAH1629 and oCAH1750. The
174 amplicon was assembled with pDS1 amplified with primers oCAH1007 and oCAH16 to generate
175 pLSQ. This plasmid was then linearized with primers oCAH1751 and oCAH16 and assembled
176 with a synthetic fragment containing a *cbbL*:c.57C>T protospacer adjacent motif (PAM)
177 mutation to generate pLSQ$^{\Delta PAM}$. The pCAH01sgRNA^{cbbL} plasmid was transferred *to M.*
178 *capsulatus* Bath harboring the pLSQ or pLSQ$^{\Delta PAM}$ strains and growth was assessed with or
179 without aTc induction using a Cell Growth Quantifier (CGQ) optical sensor (Scientific
180 Bioprocessing). High-resolution growth measurements were taken every 20 seconds with the
181 CGQ sensors, and the data is presented as the mean arbitrary light backscatter units as directly
182 detected by the sensors.
183
184 ***Design, synthesis, and construction of the M. capsulatus genome-wide sgRNA library.*** Synbio
185 Technologies designed and synthesized the sgRNA oligo pool following design rules to identify
186 15 PAM and target sequences per the predicted 3,034 open reading frames in the NC_002977.6
187 RefSeq genome and to preferentially target the non-template DNA strand within the first 50% of
188 the 5' end of the target gene. The sgRNA library consisted of 45,798 sgRNA oligos (120 bp)
189 with each containing a unique spacer sequence and 5' and 3'homologous sequence for facile
190 cloning into the p01sgRNA plasmid. The library also included 400 non-targeting sgRNAs with
191 randomly generated spacers. The pooled sgRNA library was amplified via PCR using primers
192 oCAH1020/1021 and Q5 polymerase (New England Biolabs) following the manufacturers
193 recommended reaction conditions for 14 cycles to limit biased amplification. The amplicons
194 were assembled with p01sgRNA^{mrfp} amplified with oCAH1018/1019 via isothermal assembly
195 and transformed into high-efficiency DH10b competent cells (New England Biolabs). Prior to
196 plating on selective medium, the competent cells were serially diluted to determine transformant

197 CFU/mL. Twenty antibiotic-resistant transformants were screened via PCR and Sanger
198 sequencing to determine p01sgRNA^{mrfp} background, which was < 5 %. The transformants were
199 then pooled and the library miniprepped using the Monarch Plasmid Miniprep Kit (New England
200 Biolabs). The mixed p01sgRNA library was then transferred to chemically competent S17 *E.*
201 *coli*, which were conjugated with *M. capsulatus* Bath strain with integrated P_{tet}-dCas9 to
202 generate the methanotroph CRISPRi library. *M. capsulatus* Bath transformants were quantified
203 via serial dilution plating and pooled for genomic DNA extraction and long-term -80°C storage.
204 Library composition was determined via Oxford Nanopore Technologies amplicon sequencing as
205 described below.
206
207 ***Oxford Nanopore Technologies sequencing and bioinformatic analysis.*** The sgRNA library
208 was cultivated in liquid NMS with or without CRISPRi induction. After 72 h of selection,
209 genomic DNA was extracted from an OD = 2 equivalent cell pellet using the Zymo DNA
210 extraction kit following the manufacturers protocol. 10 ng library gDNA was used as a template
211 to amplify a ~250 bp amplicon containing the sgRNA sequence with Q5 polymerase using
212 primers oCAH1020/1021 and the same reaction conditions as above (14 cycles). The amplicons
213 were barcoded with the native barcoding kit 24 V14 following the manufacturers protocol
214 (Oxford Nanopore Technologies), and sequenced on a single MinIon flow cell with high
215 accuracy basecalling, obtaining ~ 5 x 10^6 reads/sample. Sequences were then trimmed and
216 filtered using Geneious Prime software. The 20 bp sgRNA target sequences were extracted from
217 the trimmed and filtered sequence reads using a custom Python script to process Oxford
218 Nanopore Technologies sequence data stored as compressed .fasta.gz files. The script performs a
219 two-step search for the constant sgRNA sequences (TATTTTACCACTCCCTATCAGTGAT,
220 TTTTAGAGCTAGAAATAGCAAGTT or their reverse complements
221 ATCACTGATAGGGAGTGGTAAAATA, AACTTGCTATTTCTAGCTCTAAAAC) flanking
222 the target sequence and extracts the adjacent 5' or 3' 20 bp target sequence from the read
223 dependent on the identified query sequence/read strand orientation. The script utilizes pairwise
224 alignment to refine the search results, ensuring accurate extraction of relevant sequences. After
225 extraction, the sgRNA target sequences were aligned to either a custom reference library
226 containing the 45,798 sgRNA library sequences or the *M. capsulatus* Bath genome
227 (NC_002977.6); mapped reads were quantified and normalized as sgRNA target sequence per
228 million (TPM); and the fitness score (sgRNA target sequence differential abundance between
229 induced and uninduced samples) was determined following a DEseq2 workflow using Geneious
230 software. Enrichment analysis of the most differentially abundant sgRNA targets was performed
231 using ShinyGo 0.82 using the STRING database[47]
232
233 ***Illustrations.*** Data was graphed using GraphPad Prism 10 software. Circos plots were generated
234 using Circa (https://circa.omgenomics.com/). Workflow schematics were created with
235 BioRender.com.
236

Statistical analysis. Statistical analysis was performed using GraphPad Prism 10 software. The data between two groups were analyzed using unpaired t tests. Data were considered statistically significant when $p \leq 0.05$.

Results and Discussion

Construction and validation of methanotroph CRISPRi tools. We previously developed a two-plasmid, broad-host-range CRISPR-Cas9 system that enabled *M. capsulatus* genome editing [44]. This two-plasmid system consisted of a 1) pBBR-based plasmid with the *M. capsulatus* constitutive PQQ-dependent methanol dehydrogenase P_{mxaF} promoter driving single guide RNA (sgRNA) expression, and a compatible 2) IncP-based plasmid, pCAH01, with anhydrotetracycline-inducible Cas9 expression (pCAH01^{SpR}::*cas9*)[44]. To construct a broad-host-range, single plasmid CRISPRi system, we moved the P_{mxaF}-sgRNA module to pCAH01^{SpR}::*cas9* and replaced the *cas9* gene with the dead cas9 (*dcas9*) gene encoding the nuclease-deficient dCas9 variant (D10A, H840A) creating pJHCi (Figure 1a). The ability of the CRISPRi system to repress transcription in the Gammaproteobacterial methanotroph *M. capsulatus* Bath and Alphaproteobacterial methanotroph *Methylosinus trichosporium* OB3b was tested using strains expressing an mRFP reporter (Figure 1b)[48]. pJHCi with a sgRNA targeting the non-template strand of the mRFP open reading frame was transferred to the methanotroph reporter strains via conjugation. The CRISPRi system reduced *M. capsulatus* and *M. trichosporium* mRFP fluorescence by 6.3-fold and 2.3-fold, respectively, after 72 h of bacterial cultivation in liquid NMS with CH_4 as the carbon source (Figure 1c). The decreased efficiency of the CRISPRi system in *M. trichosporium* may be related to differences in sgRNA and/or dCas9 abundance as promoters derived from *Gammaproteobacteria*, like those driving transcription of the sgRNA (*M. capsulatus* P_{mxa}) and dCas9 (P_{tet}), exhibit lower activity in *M. trichosporium* compared to *M. capsulatus*[48].

The pJHCi CRISPRi system inhibited the production of fluorescent protein in the absence of dCas9 induction in both methanotrophs (Figure 1c), suggesting that low intracellular dCas9 levels from leaky P_{tet} promoter gene transcription in the context of high, constitutive sgRNA expression is sufficient for transcription repression. The leaky functionality of the CRISPRi system is not desirable for many downstream functional genomic applications where sgRNA expression could cause fitness defects during strain development. To develop a system with more tightly regulated CRISPRi repression, we designed a configuration wherein both dCas9 and the sgRNA are inducible (Figure 1d). To this end, the sgRNA^{mrfp} from pJHCi was moved to pCAH01 downstream of the P*tet* promoter for inducible sgRNA expression. We then constructed a suicide plasmid, pJHint, with the TetR-tetO inducible components flanked by *M. capsulatus* genome sequences to facilitate integration of the plasmid into an intergenic site between MCA_tRNA-Met-3 MCA_tRNA-Pro-3 via homologous recombination. dCas9 was cloned into pJHint and transferred to *M. capsulatus* to generate a strain with an aTc-inducible dCas9 gene integrated into the chromosome. We iteratively transformed the genome-integrated dCas9 *M. capsulatus* strain with the pDS1 mRFP reporter plasmid followed by the pCAH01sgRNA^{mrfp}. mRFP fluorescence in this strain was similar to a control strain with the mRFP reporter plasmid alone (Figure 1e), supporting that the CRISPRi system did not inhibit mRFP transcription in the absence of aTc induction. In contrast, simultaneous induction of dCas9 and sgRNA^{mRFP} led to a 3.3-fold decrease in mRFP fluorescence (Figure 1e). Fluorescence microscopy was used to assess CRISPRi efficiency in individual cells. As shown in Figure 1f, CRISPRi repressed mRFP fluorescence in most of the bacterial population, but some cell exhibited high mRFP fluorescence indicated a small percentage of the population may “escape” CRISPRi repression.

288 **CRISPRi-mediated transcription repression of *M. capsulatus* RubisCO causes growth**
289 **inhibition.** We previously showed that the RubisCO enzyme encoded by *M. capsulatus* is
290 essential for its growth on CH_4 [49]. As such, we targeted the *cbbL* gene encoding the RubisCO
291 large subunit to test the ability of the CRISPRi system to repress transcription from the *M.*
292 *capsulatus* chromosome. Transconjugants of the sgRNA^{cbbL} plasmid in the P_{tet}-dCas9
293 background strain could only be obtained in the absence of aTc induction (Figure 2a), supporting
294 the essentiality of RubisCO for *M. capsulatu*s growth. Transconjugants isolated in the absence of
295 CRISPRi induction were subsequently cultivated in liquid NMS with or without CRISPRi
296 induction, and high-resolution growth analysis showed that repression of *cbbL* transcription
297 significantly inhibited bacterial growth (Figure 2b). Notably, the induced culture began to grow
298 after five days and exhibited typical logarithmic growth kinetics thereafter (Figure 2b). The aTc
299 inducer has a 17 h half-life in minimal medium at pH 7 and 37°C [50], so we hypothesized that the
300 delayed growth observed in induced samples may be due to ineffective aTc concentrations after
301 five days cultivation at 37°C. However, when we subcultured the previously induced sgRNA^{cbbL}
302 culture into fresh medium with the aTc inducer we did not observe a growth defect (data not
303 shown), indicating that the CRISPRi system is no longer effective in this expanded population.
304 Cultures no longer displaying aTc-dependent growth inhibition were dilution plated on solid
305 medium to isolate "escapee" clones. The emergence of suppressor mutations that inactivate the
306 CRISPRi system tend to occur in the dCas9 gene[51]. Sanger sequencing of five "escapee"
307 colonies did not identify any nucleotide mutations in the dCas9 gene, sgRNA, P*tet-tetO*
308 promoters, or the *tetR* gene where mutations could render the CRISPRi system nonfunctional
309 (data not shown), so the underlying mechanism of resistance to CRISPRi repression in these
310 strains remains elusive. Given the essentiality of RubisCO expression, it is likely there is a strong
311 selective pressure to overcome *cbbL* transcription repression in these cells.
312
313 To further test the specificity of the CRISPRi system, we constructed a complementing plasmid
314 containing the *cbbLSQ* operon with its native promoter region (pLSQ) and another plasmid with
315 a mutated protospacer adjacent motif (PAM) next to the *cbbL* target site (MCA2743:c.57C>T,
316 pLSQ$^{\Delta PAM}$) expected to prevent dCas9 DNA binding[52,53]. (Figure 2c). CRISPRi targeting of *cbbL*
317 in the pLSQ$^{\Delta PAM}$ strain did not result in growth inhibition similar to uninduced controls (Figure
318 2d), supporting that expression of RubisCO from this plasmid was able to complement
319 chromosomal *cbbLSQ* transcription repression. In contrast, CRISPRi-mediated repression of
320 *cbbL* transcription in the strain with pLSQ inhibited bacterial growth, but not to the extent of that
321 observed in the strain lacking the plasmid (Figure 2d). The pLSQ plasmid has a pBBR-based
322 replicon, which is maintained in *M. capsulatus* at ~50 copies/cell[48]. As such, the difference in
323 growth inhibition observed between the pSLQ and control strain may be correlated to an increase
324 in target sites in cells harboring pSLQ, thereby limiting CRISPRi transcription repression
325 efficiency compared to targeting a single chromosomal site.
326
327 **CRISPRi functional genomic screening identifies genes essential for CH_4-dependent**
328 **growth.** To evaluate the utility of our CRISPRi system for functional genomic screening, we
329 designed and synthesized a pooled sgRNA library consisting of 45,798 sgRNAs, ~15 sgRNAs
330 per *M. capsulatus* protein-coding genes (3,034 annotated in the NC_002977.6 RefSeq genome)
331 and 400 non-targeting control sgRNAs (supplemental Table S1-S2). Eighteen open-reading
332 frames had less than 15 sgRNAs in the library and zero sgRNA target sequences were identified
333 for 3 genes (MCA0050, MCA0307, MCA1517, supplemental Table S3). We amplified the

334 pooled sgRNA library by PCR and cloned the amplicons into p01sgRNA via isothermal
335 assembly, replacing the sgRNA^{mrfp} targeting sequence. 1.02 x 10^7 DH10b transformants were
336 obtained after transformation, three orders of magnitude greater than the synthesized library size.
337 Colony PCR and sanger sequencing of sgRNA-containing plasmids from 20 individual
338 transformants showed that the library contained < 5 % background (sgRNA^{mrfp}). The 1 x 10^7
339 DH10b transformants were pooled and the cloned 01sgRNA library isolated by plasmid
340 miniprep. The pooled sgRNA library was then transferred to conjugative S17 *E. coli* obtaining
341 1.15 x 10^6 S17 transformants. The S17 *E. coli* was used to mobilize the library to the *M.*
342 *capsulatus* strain with a chromosomally integrated P_{tet}-dCas9 cassette via conjugation. 6.8 x 10^7
343 transconjugants were obtained, 1000X the amount of unique sgRNAs in the synthesized library.
344 We determined the library coverage at this stage by amplifying the sgRNAs from genomic DNA
345 isolated from the pooled *M. capsulatus* transconjugants. The sgRNA amplicons were sequenced
346 using Oxford Nanopore Technologies MinION; 680,425 reads with QC 12+ scores were
347 trimmed and filtered using Geneious software followed by extraction of the 20 bp sgRNA
348 targeting sequences from the processed sequences using a custom script. In total, 680,304
349 extracted sgRNA spacers were aligned to the synthesized genome-wide CRISPRi sgRNA library
350 reference with 45,554 of the 45,798 synthesized sgRNAs detected (99.5% sgRNA library
351 coverage, supplemental Table S4) with at least one sgRNA per predicted DNA coding sequence
352 (except the three genes not included in the synthesized library, supplemental Table S5) The
353 workflow for cloning and screening the sgRNA library is shown in Figure 3a.
354
355 The methanotroph genome-wide sgRNA library was cultivated in serum vials with an
356 atmosphere of 20% CH_4 in air with and without CRISPRi induction to identify genes essential
357 for *M. capsulatus* growth. We observed a minor growth defect of CRISPRi induced cultures
358 compared to uninduced cultures, but logarithmic growth kinetics and entry into stationary phase
359 were similar between the conditions (Figure 3b). The sgRNA library compositions in CRISPRi
360 induced and noninduced samples 72 h after selection were quantified by sgRNA amplicon
361 sequencing and mapping to both the synthesized sgRNA library and the *M. capsulatus* genome
362 (supplemental Tables S6-S13, read counts). We identified between 61.1-91.8% of the
363 synthesized sgRNAs in the sample sequences, with increased coverage strongly correlated to
364 sequencing depth ($R^2 = 0.93$). Although complete library coverage was not obtained in the
365 screening samples with the sequencing depth achieved here, all gene targets were represented in
366 the sequence data with 3,027/3,034 (99.8 %) of the coding DNA sequences with ≥10 guides
367 represented (supplemental Tables S6-S13). Comparing the sgRNA library composition between
368 CRISPRi induced vs noninduced samples showed that 1,019 sgRNAs were depleted (log2 fitness
369 score ≤ 1, $p \leq 0.001$) and 59 sgRNAs were enriched (log2 fitness score ≤ 1, $p \leq 0.001$) after 72
370 h of selection, presumably corresponding to a fitness defect or advantage phenotype associated
371 with transcription repression of the sgRNA target gene (Figure 4a and Table S14). Enrichment
372 analysis of 429 genes with sgRNA log2 fitness scores ≤ -3 and probability values ≤ 0.001
373 indicated they encode proteins associated with essential cellular processes like translation,
374 transcription, ribosome biosynthesis, and amino acid and nucleotide biosynthesis (Figure 4b and
375 Table S15). Enrichment analysis of the genes whose transcription repression resulted in a fitness
376 advantage did not enrich any pathways. Notably, 99.5% (398/400) of the non-targeting control
377 sgRNAs did not have significant differential fitness scores (log2 ≤-1 or ≥1, $p \leq 0.001$) between
378 the two conditions (supplemental Table S14).
379

380 Several sgRNAs targeting known central CH_4 metabolic enzyme genes had significant negative
381 fitness scores (Figure 4c and supplemental Table S14), including those targeting the particulate
382 methane monooxygenase operons (MCA1796-98 and MCA2853-55), the calcium- and PQQ-
383 dependent methanol dehydrogenase (MCA0779), and the RuMP cycle operons (MCA3040-45
384 and 3046-50). As expected based on our initial CRISPRi experiments (Figure 2), sgRNAs
385 targeting the *cbbLSQ* operon (MCA2743-46) were among those with the lowest fitness scores.
386 Further, the sgRNAs targeting the Entner-Doudoroff pathway *edd* and *eda* genes (MCA0037-38)
387 were significantly depleted in the screen, consistent with biochemical data and genome-scale
388 models predicting this pathway to be essential and the primary route for pyruvate biosynthesis in
389 *M. capsulatus* Bath[5,54,55]. Also, the depletion of sgRNAs targeting the tetrahydromethanopterin
390 formaldehyde dissimilatory pathway corroborate flux balance model predictions that this is the
391 primary route used by *M. capsulatus* for formaldeyde conversion to formate[54,55]. Notably,
392 sgRNAs targeting genes encoding serine cycle enzymes showed no differential fitness during
393 growth on CH_4.
394
395 Many sgRNAs targeting the same gene or genes within operons exhibited similar fitness scores,
396 highlighting the potential of the CRISPRi library and screening pipeline to identify functional
397 gene targets (supplemental Table S14). For example, sgRNAs targeting ribosomal protein operon
398 genes MCA2368, MCA2371, MCA2372, and MCA2374 were consistently depleted under
399 CRISPRi induction conditions with log2 fitness scores of -5.47, -5.57, -5.70, and -6.37,
400 respectively, while sgRNAs targeting the cobalt transporter and cobalamin biosynthetic operon
401 genes MCA2300, MCA2301, and MCA2302 were significantly enriched with log2 fitness scores
402 of 3.10, 2.70 and 3.65, respectively. However, significant fitness score variances between
403 sgRNAs targeting the same gene were observed, suggesting CRISPRi effectiveness to repress
404 transcription can vary depending on the target site. Further evaluation of the individual *pmoCAB*-
405 and *cbbLSQ*-targeting sgRNAs showed highly variable fitness scores, especially those targeting,
406 *pmoC*, *pmoA*, and the *cbbL* genes (supplemental Figure S1).
407
408 We next mapped the sgRNA target sequences from CRISPRi induced and noninduced cultures to
409 the *M. capsulatus* Bath genome to determine overall sgRNA/gene fitness. Given the size of the
410 sgRNA library and multiple sgRNAs per ORF, only those genes with consistent positive or
411 negative sgRNA fitness scores were expected to be identified in the analysis. We identified 233
412 genes whose transcription repression resulted in a fitness defect (sgRNAs depleted in the induced
413 samples, $\log2 \leq -1$, $p \leq 0.001$) and repression of 13 genes associated with a fitness advantage
414 (sgRNAs enriched in the induced samples, $\log2 \geq 1$, $p \leq 0.001$) (Figure 5a and supplemental
415 Table S16). Enrichment analysis of the 233 genes with significant sgRNA log2 fitness scores ≤ -
416 1 linked the genes to the essential processes of translation, transcription, ribosome biosynthesis,
417 and amino acid and nucleotide biosynthesis (Figure 5b and supplemental Table S17), consistent
418 with the analysis using the sgRNA reference library. The *edd* gene encoding the ED pathway 6-
419 phosphogluconate dehydratase had the largest differential fitness score (log2 = -3.9, $p = 1.63e^{-71}$,
420 Table 3). Several putative essential genes are involved in antioxidant defenses, Fe-S cluster
421 assembly/repair, and disulfide reduction, including superoxide dismutase (MCA2458, log2 -3.2),
422 a putative Rnf electron transport complex (MCA2893-2899, log2 -3.1), ferredoxin (MCA2470,
423 log2 -3.0), and thioredoxin disulfide reductase (MCA1694, log2-2.6). These genes may be
424 involved in balancing redox homeostasis during CH_4 oxidation[56,57], and represent gene targets
425 for downstream gene-function analysis. sgRNAs targeting genes in the cobalamin biosynthetic

426 operon (MCA2290-MCA2302) had consistent positive fitness scores and MCA2302, putatively
427 encoding a putative CbtB subunit of a cobalt transporter, was identified as significantly enriched
428 (log2 = 1.26, $p = 3.9e^{-11}$) when mapping all sgRNAs to the *M. capsulatus* genome (Table 3 and
429 supplemental Table S16). Additional inquiry is required to provide insight into the underlying
430 molecular mechanism(s) linking inhibition of cobalt transport/cobalamin biosynthesis to
431 improved fitness. As expected based on the variable fitness scores for sgRNAs targeting the
432 pMMO and RubisCO operons, only the *cbbS* (encoding the RubisCO small subunit) and *cbbQ*
433 (encoding a putative RubisCO activase) genes with consistent sgRNA scores were associated
434 with negative fitness scores when mapping to the genome. Interestingly, another putative
435 RubisCO activase gene (MCA2754, log2 = -3.1, $p = 2.4e^{-22}$) may be essential for *M. capsulatus*
436 growth on CH_4. Evaluating the RubisCO activases under differential growth conditions may
437 provide insight into their roles in methanotrophic growth of *M. capsulatus*.
438
439 To validate our screening results, we used the CRISPRi system to individually target five genes
440 with significant negative fitness scores involved in *M. capsulatus* central metabolism (*edd*,
441 MCA0037, encoding phosphogluconate dehydratase of the Entner-Doudoroff pathway); DNA
442 replication (*dnaA*, MCA2470, encoding the DNA replication initiator), redox metabolism (*fdx*,
443 MCA2470, encoding a ferredoxin; ribosome biogenesis (r*psB*, MCA0567, encoding the S2
444 protein component of the ribosome 30S subunit); and amino acid biosynthesis (*asnB*, MCA2127,
445 encoding the asparagine synthase) (Table 3). Consistent with the screening results, high-
446 resolution growth analysis of *M. capsulatus* strains expressing individual sgRNAs displayed
447 significantly inhibited growth compared to uninduced controls or a non-targeting sgRNA (Figure
448 6a-f). Similar to that observed when targeting the *cbbL* gene (Figure 2), these strains evolved to
449 overcome CRISPRi-mediated growth inhibition and began to expand after several days of
450 selective pressure. Nonetheless, these data validate that the CRISPRi system developed here is
451 effective for functional genomic screening and identification of genes required for CH_4-
452 dependent growth.
453
454 **Conclusions**
455 Collectively, our results demonstrate that the CRISPRi system developed here can be used for
456 targeted transcription repression in phylogenetically diverse methanotrophic bacteria. Selective
457 screening of a genome-wide sgRNA library during CH_4-dependent cultivation identified
458 predicted and novel essential genes required for methanotrophic growth. The CRISPRi system
459 and associated datasets herein will serve as valuable resources for hypothesis-driven inquiry into
460 genes required for methanotrophy. Additionally, targeted sgRNA libraries can be improved by
461 selecting sgRNAs with the most consistent differential fitness scores. We also expect that these
462 CRISPRi tools can be coupled with other synthetic biology approaches to optimize
463 methanotrophic strains for carbon- and energy-efficient CH_4 capture and conversion.

References

1. Guerrero-Cruz, S. et al. Methanotrophs: discoveries, environmental relevance, and a perspective on current and future applications. Front. Microbiol. 12, 678057 (2021).
2. Lidstrom, M. E. Direct Methane Removal from Air by Aerobic Methanotrophs. Cold Spring Harb. Perspect. Biol. 16, (2024).
3. Tucci, F. J. & Rosenzweig, A. C. Direct Methane Oxidation by Copper- and Iron-Dependent Methane Monooxygenases. Chem. Rev. 124, 1288–1320 (2024).
4. Kalyuzhnaya, M. G., Gomez, O. A. & Murrell, J. C. The Methane-Oxidizing Bacteria (Methanotrophs). in Taxonomy, Genomics and Ecophysiology of Hydrocarbon-Degrading Microbes (ed. McGenity, T. J.) 1–34 (Springer International Publishing, 2019). doi:10.1007/978-3-319-60053-6_10-1.
5. Strom, T., Ferenci, T. & Quayle, J. R. The carbon assimilation pathways of Methylococcus capsulatus, Pseudomonas methanica and Methylosinus trichosporium (OB3B) during growth on methane. Biochem. J. 144, 465–476 (1974).
6. Heptinstall, J. & Quayle, J. R. Pathways leading to and from serine during growth of Pseudomonas AM1 on C1 compounds or succinate. Biochem. J. 117, 563–572 (1970).
7. Lawrence, A. J., Kemp, M. B. & Quayle, J. R. Synthesis of cell constituents by methane-grown Methylococcus capsulatus and Methanomonas methanooxidans. Biochem. J. 116, 631–639 (1970).
8. Chistoserdova, L., Vorholt, J. A., Thauer, R. K. & Lidstrom, M. E. C1 transfer enzymes and coenzymes linking methylotrophic bacteria and methanogenic Archaea. Science 281, 99–102 (1998).
9. Vorholt, J. A. Cofactor-dependent pathways of formaldehyde oxidation in methylotrophic bacteria. Arch. Microbiol. 178, 239–249 (2002).
10. Kalyuzhnaya, M. G. et al. Highly efficient methane biocatalysis revealed in a methanotrophic bacterium. Nat. Commun. 4, 2785 (2013).
11. Vuilleumier, S. et al. Genome sequence of the haloalkaliphilic methanotrophic bacterium Methylomicrobium alcaliphilum 20Z. J. Bacteriol. 194, 551–552 (2012).
12. Mateos-Rivera, A., Islam, T., Marshall, I. P. G., Schreiber, L. & Øvreås, L. High-quality draft genome of the methanotroph Methylovulum psychrotolerans Str. HV10-M2 isolated from plant material at a high-altitude environment. Stand. Genomic Sci. 13, 10 (2018).
13. Miroshnikov, K. K. et al. Draft Genome Sequence of Methylocapsa palsarum NE2T, an Obligate Methanotroph from Subarctic Soil. Genome Announc. 5, (2017).
14. Kalyuzhnaya, M. G. et al. Draft genome sequences of gammaproteobacterial methanotrophs isolated from lake washington sediment. Genome Announc. 3, (2015).
15. Hamilton, R. et al. Draft genomes of gammaproteobacterial methanotrophs isolated from terrestrial ecosystems. Genome Announc. 3, (2015).
16. Orata, F. D., Kits, K. D. & Stein, L. Y. Complete Genome Sequence of Methylomonas denitrificans Strain FJG1, an Obligate Aerobic Methanotroph That Can Couple Methane Oxidation with Denitrification. Genome Announc. 6, (2018).

505 17. Oshkin, I. Y. et al. Complete Genome Sequence of Methylococcus capsulatus MIR, a
506 Methanotroph Capable of Growth on Methanol. Microbiol. Resour. Announc. 11, e0054222
507 (2022).
508 18. Stein, L. Y. et al. Genome sequence of the obligate methanotroph Methylosinus
509 trichosporium strain OB3b. J. Bacteriol. 192, 6497–6498 (2010).
510 19. Van Dien, S. J. et al. Reconstruction of C(3) and C(4) metabolism in Methylobacterium
511 extorquens AM1 using transposon mutagenesis. Microbiology (Reading, Engl) 149, 601–609
512 (2003).
513 20. Marx, C. J., O'Brien, B. N., Breezee, J. & Lidstrom, M. E. Novel methylotrophy genes of
514 Methylobacterium extorquens AM1 identified by using transposon mutagenesis including a
515 putative dihydromethanopterin reductase. J. Bacteriol. 185, 669–673 (2003).
516 21. Lee, K. E., Stone, S., Goodwin, P. M. & Holloway, B. W. Characterization of transposon
517 insertion mutants of Methylobacterium extorquens AM1 (Methylobacterium strain AM1) which
518 are defective in methanol oxidation. Microbiology (1991).
519 22. Chistoserdova, L. Metabolism of Formaldehyde in M. extorquens AM1: Molecular
520 genetic analysis and mutant characterization. in Microbial growth on C1 compounds (eds.
521 Lidstrom, M. E. & Tabita, F. R.) 16–24 (Springer Netherlands, 1996). doi:10.1007/978-94-009-
522 0213-8_4.
523 23. Vorholt, J. A., Marx, C. J., Lidstrom, M. E. & Thauer, R. K. Novel formaldehyde-
524 activating enzyme in Methylobacterium extorquens AM1 required for growth on methanol. J.
525 Bacteriol. 182, 6645–6650 (2000).
526 24. Nunn, D. N. & Lidstrom, M. E. Phenotypic characterization of 10 methanol oxidation
527 mutant classes in Methylobacterium sp. strain AM1. J. Bacteriol. 166, 591–597 (1986).
528 25. Springer, A. L., Chou, H. H., Fan, W. H., Lee, E. & Lidstrom, M. E. Methanol oxidation
529 mutants in Methylobacterium extorquens AM1: identification of new genetic complementation
530 groups. Microbiology (Reading, Engl) 141 (Pt 11), 2985–2993 (1995).
531 26. Whitta, S., Sinclair, M. I. & Holloway, B. W. Transposon Mutagenesis in
532 Methylobacterium AM1 (Pseudomonas AM1). Microbiology (1985).
533 27. Roszczenko-Jasińska, P. et al. Gene products and processes contributing to lanthanide
534 homeostasis and methanol metabolism in Methylorubrum extorquens AM1. Sci. Rep. 10, 12663
535 (2020).
536 28. Ochsner, A. M. et al. Transposon sequencing uncovers an essential regulatory function of
537 phosphoribulokinase for methylotrophy. Curr. Biol. 27, 2579-2588.e6 (2017).
538 29. Groom, J. D., Ford, S. M., Pesesky, M. W. & Lidstrom, M. E. A Mutagenic Screen
539 Identifies a TonB-Dependent Receptor Required for the Lanthanide Metal Switch in the Type I
540 Methanotroph "Methylotuvimicrobium buryatense" 5GB1C. J. Bacteriol. 201, (2019).
541 30. Sharpe, P. L. et al. Use of transposon promoter-probe vectors in the metabolic
542 engineering of the obligate methanotroph Methylomonas sp. strain 16a for enhanced C40
543 carotenoid synthesis. Appl. Environ. Microbiol. 73, 1721–1728 (2007).

544 31. Cheng, M., Pei, D., He, L., Fei, Q. & Yan, X. Cre/lox-Mediated CRISPRi Library
545 Reveals Core Genome of a Type I Methanotroph Methylotuvimicrobium buryatense 5GB1C.
546 Appl. Environ. Microbiol. 89, e0188322 (2023).
547 32. Hawkins, J. S., Wong, S., Peters, J. M., Almeida, R. & Qi, L. S. Targeted transcriptional
548 repression in bacteria using CRISPR interference (crispri). Methods Mol. Biol. 1311, 349–362
549 (2015).
550 33. de Bakker, V., Liu, X., Bravo, A. M. & Veening, J.-W. CRISPRi-seq for genome-wide
551 fitness quantification in bacteria. Nat. Protoc. 17, 252–281 (2022).
552 34. Hawkins, J. S. et al. Mismatch-CRISPRi Reveals the Co-varying Expression-Fitness
553 Relationships of Essential Genes in Escherichia coli and Bacillus subtilis. Cell Syst. 11, 523-
554 535.e9 (2020).
555 35. Yao, L. et al. Pooled CRISPRi screening of the cyanobacterium Synechocystis sp PCC
556 6803 for enhanced industrial phenotypes. Nat. Commun. 11, 1666 (2020).
557 36. Shin, J. et al. Genome-wide CRISPRi screen identifies enhanced autolithotrophic
558 phenotypes in acetogenic bacterium Eubacterium limosum. Proc Natl Acad Sci USA 120,
559 e2216244120 (2023).
560 37. Mo, X.-H. et al. Establishment of CRISPR interference in Methylorubrum extorquens
561 and application of rapidly mining a new phytoene desaturase involved in carotenoid
562 biosynthesis. Appl. Microbiol. Biotechnol. 104, 4515–4532 (2020).
563 38. Wang, T. et al. Pooled CRISPR interference screening enables genome-scale functional
564 genomics study in bacteria with superior performance. Nat. Commun. 9, 2475 (2018).
565 39. Jiang, W., Oikonomou, P. & Tavazoie, S. Comprehensive Genome-wide Perturbations
566 via CRISPR Adaptation Reveal Complex Genetics of Antibiotic Sensitivity. Cell 180, 1002-
567 1017.e31 (2020).
568 40. Qi, L. S. et al. Repurposing CRISPR as an RNA-guided platform for sequence-specific
569 control of gene expression. Cell 152, 1173–1183 (2013).
570 41. Enright, A. L., Heelan, W. J., Ward, R. D. & Peters, J. M. CRISPRi functional genomics
571 in bacteria and its application to medical and industrial research. Microbiol. Mol. Biol. Rev. 88,
572 e0017022 (2024).
573 42. Rumah, B. L. et al. In vivo genome editing in type I and II methanotrophs using a
574 crispr/cas9 system. ACS Synth. Biol. 12, 544–554 (2023).
575 43. Jeong, J. et al. A highly efficient and versatile genetic engineering toolkit for a
576 methanotroph-based biorefinery. Chemical Engineering Journal 453, 139911 (2023).
577 44. Tapscott, T., Guarnieri, M. T. & Henard, C. A. Development of a CRISPR/Cas9 System
578 for Methylococcus capsulatus In Vivo Gene Editing. Appl. Environ. Microbiol. 85, (2019).
579 45. Nath, S., Henard, J. M. & Henard, C. A. Optimized tools and methods for methanotroph
580 genome editing. Methods Mol. Biol. 2489, 421–434 (2022).
581 46. Emelianov, G. et al. Engineered Methylococcus capsulatus Bath for efficient methane
582 conversion to isoprene. Bioresour. Technol. 393, 130098 (2024).

583 47. Ge, S. X., Jung, D. & Yao, R. ShinyGO: a graphical gene-set enrichment tool for animals
584 and plants. Bioinformatics 36, 2628–2629 (2020).
585 48. Bhat, E. H. et al. Construction of a broad-host-range Anderson promoter series and
586 particulate methane monooxygenase promoter variants expand the methanotroph genetic
587 toolbox. Synthetic and Systems Biotechnology 9, 250–258 (2024).
588 49. Henard, C. A. et al. Ribulose-1,5-Bisphosphate Carboxylase/Oxygenase (RubisCO) Is
589 Essential for Growth of the Methanotroph Methylococcus capsulatus Strain Bath. Appl. Environ.
590 Microbiol. 87, e0088121 (2021).
591 50. Politi, N. et al. Half-life measurements of chemical inducers for recombinant gene
592 expression. J. Biol. Eng. 8, 5 (2014).
593 51. Zhao, H. et al. Depletion of Undecaprenyl Pyrophosphate Phosphatases Disrupts Cell
594 Envelope Biogenesis in Bacillus subtilis. J. Bacteriol. 198, 2925–2935 (2016).
595 52. Sternberg, S. H., Redding, S., Jinek, M., Greene, E. C. & Doudna, J. A. DNA
596 interrogation by the CRISPR RNA-guided endonuclease Cas9. Nature 507, 62–67 (2014).
597 53. Wu, X. et al. Genome-wide binding of the CRISPR endonuclease Cas9 in mammalian
598 cells. Nat. Biotechnol. 32, 670–676 (2014).
599 54. Gupta, A. et al. Genome-scale metabolic reconstruction and metabolic versatility of an
600 obligate methanotroph Methylococcus capsulatus str. Bath. PeerJ 7, e6685 (2019).
601 55. Lieven, C. et al. A Genome-Scale Metabolic Model for Methylococcus capsulatus (Bath)
602 Suggests Reduced Efficiency Electron Transfer to the Particulate Methane Monooxygenase.
603 Front. Microbiol. 9, 2947 (2018).
604 56. Jouanneau, Y., Jeong, H. S., Hugo, N., Meyer, C. & Willison, J. C. Overexpression in
605 Escherichia coli of the rnf genes from Rhodobacter capsulatus--characterization of two
606 membrane-bound iron-sulfur proteins. Eur. J. Biochem. 251, 54–64 (1998).
607 57. Alleman, A. B. & Peters, J. W. Mechanisms for Generating Low Potential Electrons
608 across the Metabolic Diversity of Nitrogen-Fixing Bacteria. Appl. Environ. Microbiol. 89,
609 e0037823 (2023).

Acknowledgements
This work was supported by a BioDiscovery Institute Seed Grant to CH and RA, the Department of Energy via contract with the MSI STEM Research & Development Consortium (MSRDC) to CH, and the National Science Foundation MCB award # 2225776 to CH. We would like to thank Tallon Coxe in the Azad laboratory for computational support with initial sgRNA library design.

Author Contributions
CH conceived the project. JH, SL, and YCY performed experiments. CH acquired funding, analyzed and graphed data, and provided overall guidance. CH wrote the manuscript. All others edited and approved the manuscript.

Data Availability
Plasmids will be available at Addgene upon publication. ONT sequencing data will be deposited at the NCBI Sequence Read Archive (SRA) prior to publication. Code for sgRNA target sequence extraction can be downloaded from the Henard laboratory GitHub database (https://github.com/HenardLab).

Figures and Legends

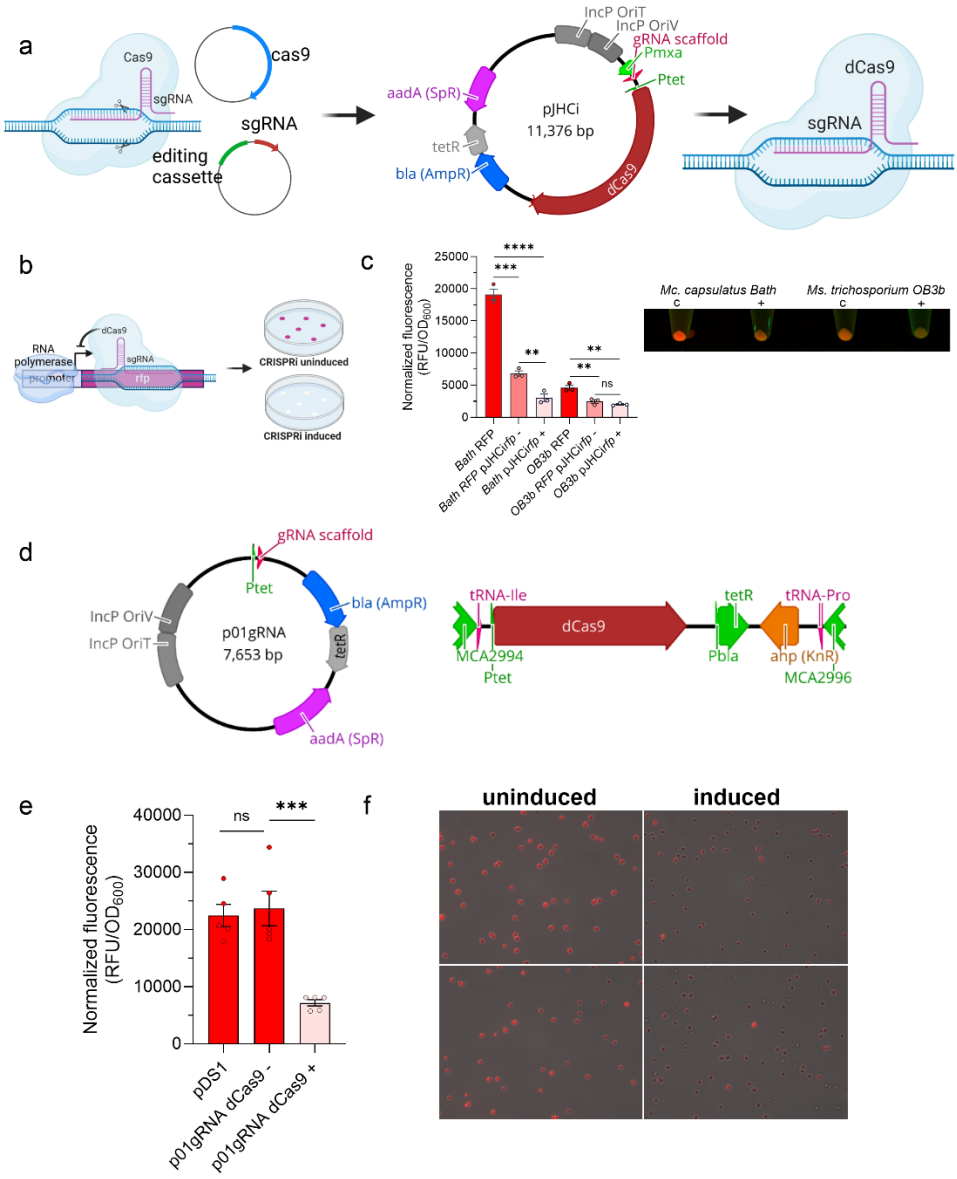

Figure 1. Construction and validation of a methanotroph CRISPRi system. a) Schematic overview of converting a two-plasmid CRISPR genome editing system into a single-plasmid CRISPRi system for targeted repression of gene expression. b and c) The mRFP fluorescent reporter was used as a read-out of CRISPRi functionality in Gammaproteobacterial methanotroph *Methylococcus capsulatus* Bath and Alphaproteobacterial methanotroph *Methylosinus trichosporium* OB3b with (+) or without (-) dCas9 induction by anhydrotetracycline (aTc). A representative image of cell pellets is shown in (c) d) The pJHCi single plasmid system exhibited leaky functionality, so an *M. capsulatus* Bath strain was generated with an aTc-inducible dCas9 cassette integrated into the chromosome and plasmid with aTc-inducible sgRNA expression. e) mRFP fluorescence with or without aTc induction

639 compared to the pDS1 mRFP reporter plasmid control strain showing tightly regulated CRISPRi
640 gene transcription repression. f) Fluorescence microscopy of *M. capsulatus* with or without
641 CRISPRi induction for mRFP repression. Representative images from biological replicates are
642 shown. Data in c and e represent the mean ± SEM from two independent experiments (n=3-5).
643 ** $p \leq 0.01$, *** $p \leq 0.001$, **** $p \leq 0.0001$.

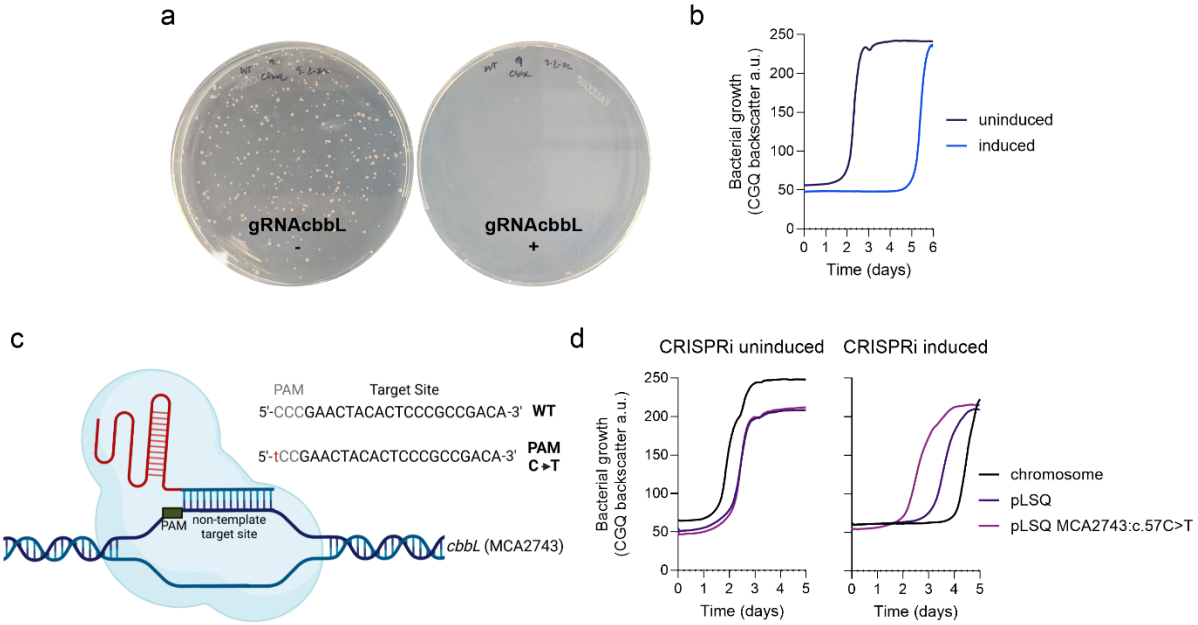

Figure 2. CRISPRi-mediated transcription repression of the genes encoding the essential ribulose 1,5 bisphosphate carboxylase/oxygenase (RubisCO) enzyme limit *M. capsulatus* growth. Growth of *M. capsulatus* with (+) or without (-) induction of dCas9 and an sgRNA targeting the *cbbL* gene encoding the large subunit of RubisCO on solid NMS medium (a) or in liquid NMS medium in a serum vial over time (b) with a 20% CH_4 in air atmosphere. c) A complementing plasmid expressing the *cbbLSQ* operon (pLSQ) was constructed and the protospacer adjacent motif (PAM) site in the *cbbL* target sequence (MCA2743) was mutated (c57C>T). d) Growth of strains carrying the pLSQ or $pLSQ^{\Delta PAM}$ compared to an isogenic background control strain with or without CRISPRi induction. Data in b and d represent the means of two independent high-resolution cultivation experiments (n=6).

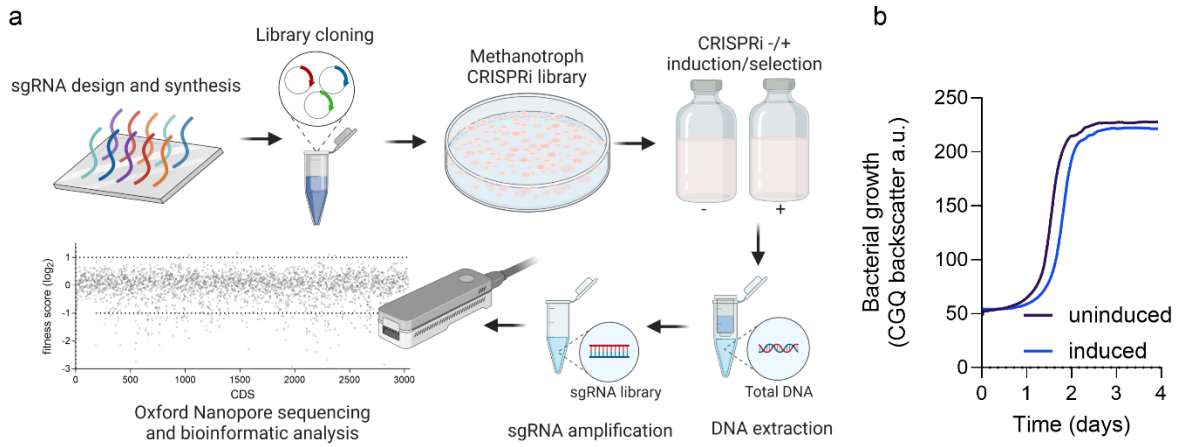

Figure 3. CRISPRi library construction and screening. a) 45,798 sgRNAs were synthesized via massively parallel oligonucleotide synthesis and cloned into the inducible plasmid pCAH01 to generate a cloned sgRNA library. The sgRNA library was transferred to an *M. capsulatus* Bath strain with a chromosomally integrated P_{tet}-dCas9 cassette via biparental mating. b) The library was cultivated with or without sgRNA and dCas9 induction in NMS medium in serum vials with a 20% CH_4 in air atmosphere. After selection, the sgRNA composition and abundances were determined via Oxford Nanopore Technologies amplicon sequencing and bioinformatic analysis to quantify sgRNA fitness. Data in b represent the means of two independent high-resolution cultivation experiments (n=6).

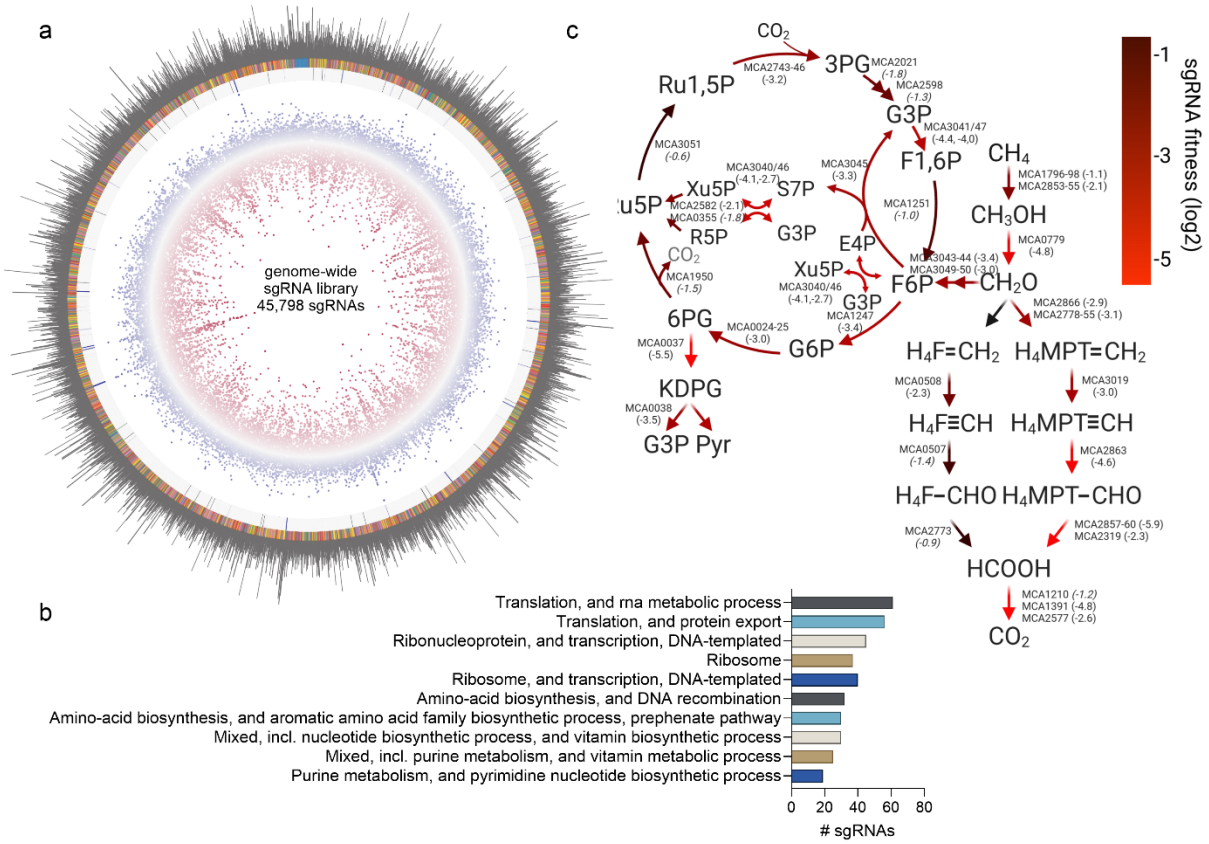

Figure 4. A CRISPRi genome-wide screen identifies genes essential for CH_4-dependent growth of *M. capsulatus*: mapping to the sgRNA library. a) Circos plot of the methanotroph sgRNA library raw reads (outer ring) mapped to the 45,798 synthesized sgRNA oligos (rainbow ring with non-targeting sgRNAs in blue). Differential sgRNA fitness scores determined via DeSeq2 between CRISPRi induced and uninduced samples during selection/cultivation with CH_4 as the sole carbon and energy source (4th ring, blue dots log2 >1; red dots log2 <1). sgRNAs depleted in the screen (negative fitness scores) correspond to genes with transcription repression causing a growth defect where those enriched (positive fitness scores) correspond to genes with transcription repression causing a growth advantage. sgRNAs with statistically significant ($p \leq 0.01$) differential fitness scores are indicated (blue squares, 3rd ring). b) ShinyGo enrichment analysis of the 429 genes with sgRNA log2 fitness scores ≤ -3 and $p \leq 0.001$. c) CH_4 assimilatory and dissimilatory metabolic pathways predicted by sgRNA fitness scores. The mean sgRNA fitness scores are indicated in parentheses next to the gene loci that encode metabolic enzymes. Scores with $p \geq 0.01$ are italicized.

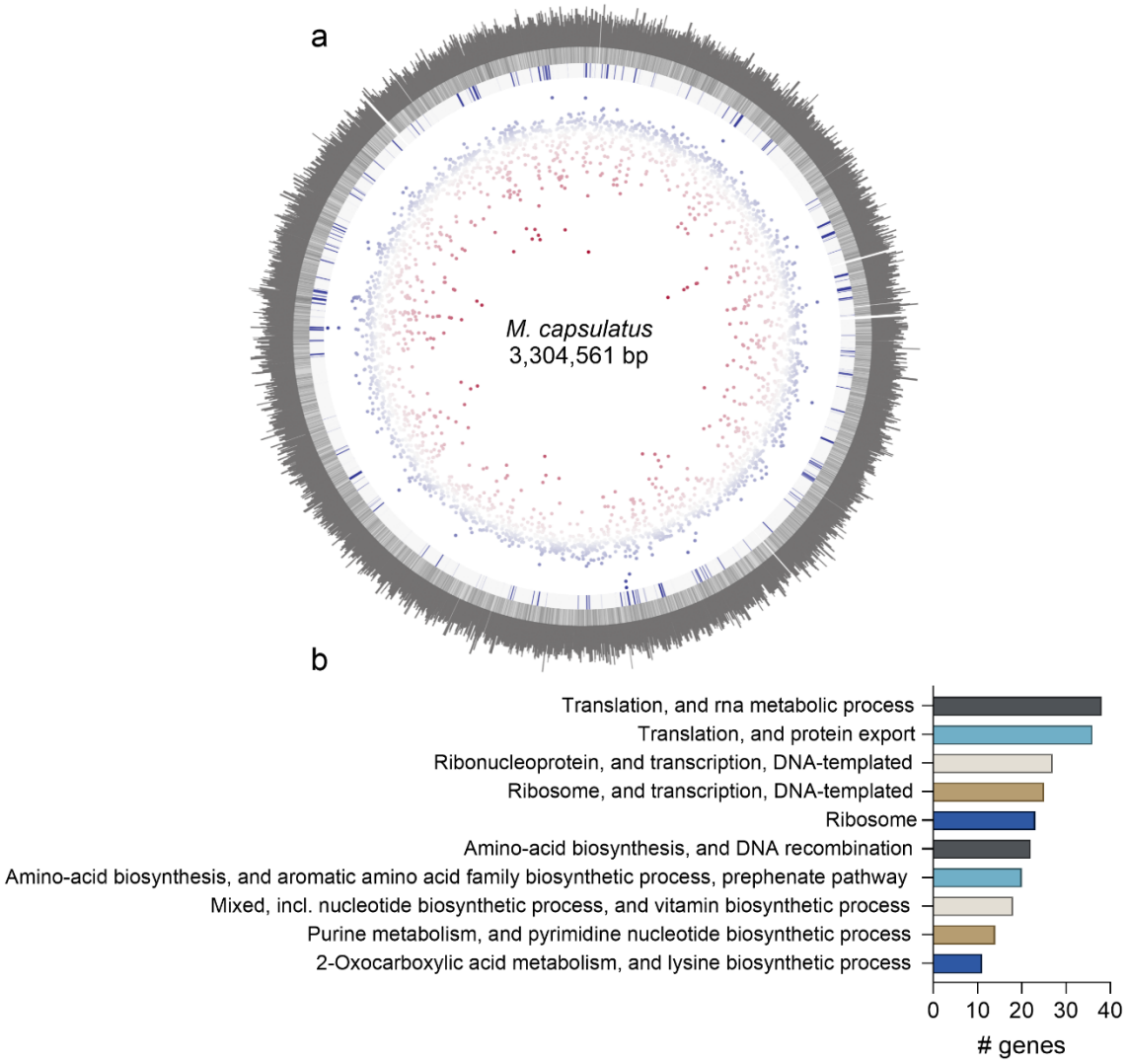

Figure 5. A CRISPRi genome-wide screen identifies genes essential for CH_4-dependent growth of *M. capsulatus*: mapping to the *M. capsulatus* genome. a) Circos plot of the methanotroph sgRNA library raw reads (outer ring) mapped to the NC_002977 *M. capsulatus* reference genome (2nd ring, genes in forward direction are in dark grey and reverse direction in light grey). Differential sgRNA fitness scores determined via DeSeq2 between CRISPRi induced and uninduced samples during selection/cultivation with CH_4 as the sole carbon and energy source (4th ring, blue dots log2 >1; red dots log2 <1). sgRNAs depleted in the screen (negative fitness scores) correspond to genes with transcription repression causing a growth defect where those enriched (positive fitness scores) correspond to genes with transcription repression causing a growth advantage. sgRNAs with statistically significant ($p \leq 0.01$) differential fitness scores are indicated (blue squares, 3rd ring). b) ShinyGo enrichment analysis of the 233 genes with sgRNA log2 fitness scores ≤ -1 and $p \leq 0.001$

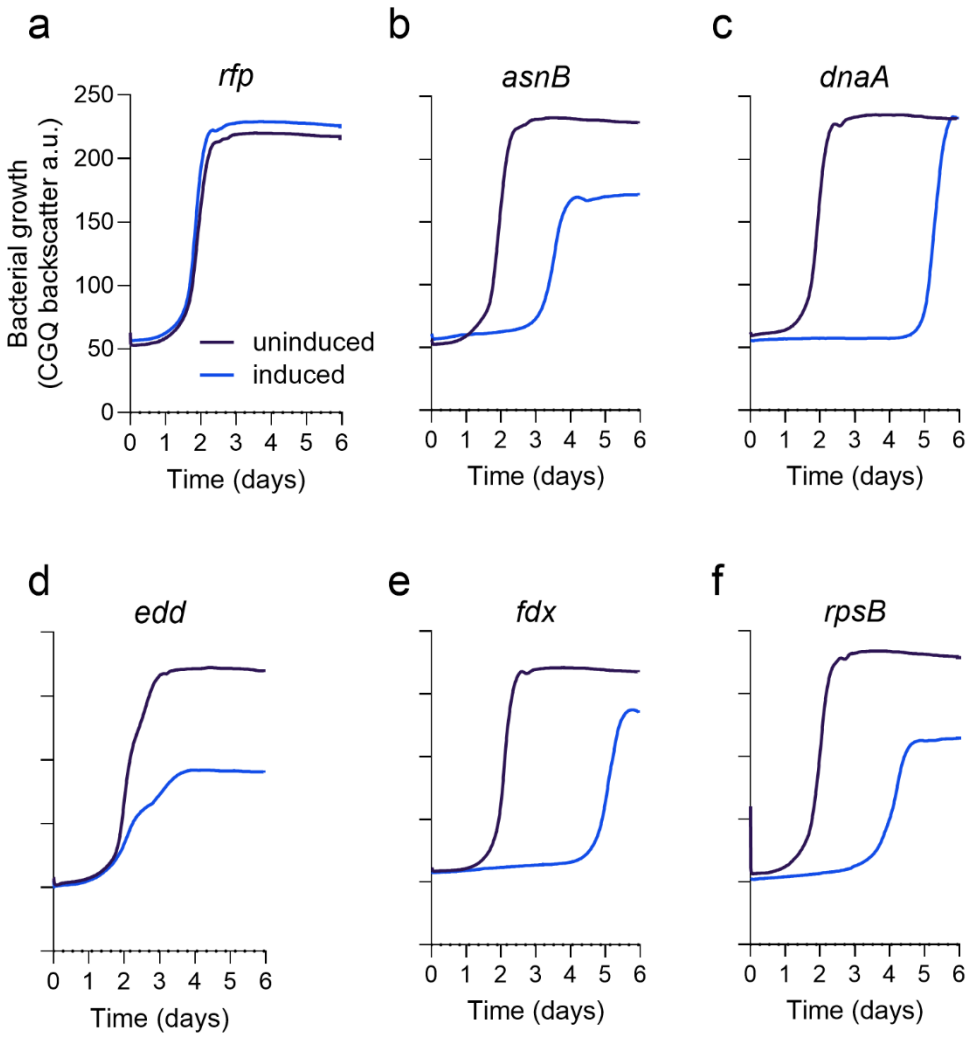

694
695 **Figure 6. CRISPRi targeted transcription repression of putative essential genes inhibits**
696 **CH_4-dependent growth.** a-f) High resolution growth curves of strains with sgRNAs targeting
697 genes identified in the genome-wide screen as essential for CH_4-dependent growth with (blue
698 line) or without (purple line) CRISPRi induction in NMS medium in serum vials with 20% CH_4
699 in air atmosphere. A strain expressing an sgRNA targeting mRFP was included as a control (a).
700 Genes represent those encoding enzymes involved in amino acid biosynthesis (b, *asnB*,
701 MCA2127); DNA replication (c, *dnaA*, MCA3033); CH4 assimilation (d, *edd*, MCA0037);
702 redox homeostasis (e, *fdx*, MCA2470); and ribosome biosynthesis (f, *rpsB*, MCA0567). Data
703 represent the means of two independent high-resolution cultivation experiments (n=6).

704 **Tables**

705

Table 1. Strains and Plasmids		
Name	**Genotype**	**Source**
***Methylococcus capsulatus* Bath**	Wild-type	Lab stock (originating from Kalyuzhnaya lab)
CH2236	*M. capsulatus* Bath with pDS1	Bhat et al[48]
CH2484	*M. capsulatus* Bath with pDS1 and pJHCi	This study
CH2486	*M. capsulatus* Bath with pJH1 and pJHCi^{sfgfp}	This study
CH2342	*M. capsulatus* Bath with inducible dCas9 integrated into the chromosome	This study
CH2475	CH2342 with p01sgRNA^{mrfp}	This study
CH2473	CH2342 with p01sgRNA^{cbbL}	This study
CH2529	CH2342 with p01sgRNA^{gwlibrary}	This study
CH2537	CH2342 with p01sgRNA^{MCA2127}	This study
CH24077	CH2342 with p01sgRNA^{MCA3033}	This study
CH2535	CH2342 with p01sgRNA^{MCA0037}	This study
CH24076	CH2342 with p01sgRNA^{MCA2470}	This study
CH2536	CH2342 with p01sgRNA^{MCA0567}	This study
***Methylosinus trichosporium* OB3b**	Wild-type	[18]
CH2507	*M. trichosporium* OB3b with pDS1	Bhat et al[48]
CH2508	*M. trichosporium* OB3b with pDS1 and pJHCi	This study
***Escherichia coli* Zymo 10B**	F- *mcrA* Δ(*mrr-hsdRMS-mcrBC*) Φ80*lacZ*ΔM15 Δ*lacX*74 *recA1 endA1 araD139* Δ(*ara leu*) 7697 *galU galK rpsL nupG*	Zymo Research
***E. coli* S17-1**	Tp^r Sm^r *recA thi pro hsd*(r$^-$m$^+$)RP4-2-Tc::Mu::Km Tn7	ATCC 47055
Plasmids		
Name	**Description**	**Source**
pCAH01^{SpR}	IncP broad-host-range inducible expression plasmid	Addgene #128159[44]
pCAH01^{SpR}::Cas9	Inducible Cas9 expression	Addgene #128160[44]
pdCas9-bacteria	aTc-inducible expression of catalytically inactive *S. pyogenes* Cas9 (dCas9)	Addgene #44249[40]
pDS1	pBBR1MCS-5 with BBa_J23119-mRFP reporter	Bhat et al[48]
pJHCi	pCAH01^{SpR}::Cas9 *cas9* gene replaced with *dcas9* and *M. capsulatus* P_{mxa} driving expression of mRFP targeting sgRNA	This study

pJHint	*tetO*-TetR inducible suicide plasmid that integrates into the *M. capsulatus* genome between MCA and MCA.	This study
pJHint::dCas9	pJHint with dCas9 gene for chromosomal integration of inducible dCas9 cassette	This study
pLSQ	*M. capsulatus cbbLSQ* operon with native promoter cloned into pBMTL-2	This study
pL$^{PAMC>T}$SQ	pCbbLSQ with mutated PAM site	This study
p01sgRNA^{mrfp}	pCAH01 with sgRNA targeting mRFP ORF	This study
p01sgRNA^{cbbL}	pCAH01 with sgRNA targeting MCA2743 (*cbbL*) ORF	This study
p01sgRNA^{MCA2127}	pCAH01 with sgRNA targeting MCA2127 (*asnB*) ORF	This study
p01sgRNA^{MCA3033}	pCAH01 with sgRNA targeting MCA3033 (*dnaA*) ORF	This study
p01sgRNA^{MCA0037}	pCAH01 with sgRNA targeting MCA0037 (*edd*) ORF	This study
p01sgRNA^{MCA2470}	pCAH01 with sgRNA targeting MCA2470 (*fdx*) ORF	This study
p01sgRNA^{MCA0567}	pCAH01 with sgRNA targeting MCA0567 (*rpsB*) ORF	This study

706

Table 2. Primers and synthetic DNA fragments	
Name	**Sequence**
Construction of pJHCi	
oCAH230 pCAH01^{SpR}::Cas9 F	GTTCTTTCCTGCGTTATCCC
oCAH231 pCAH01^{SpR}::Cas9 R	GTCTGACGCTCAGTGGAA
oCAH267 P_{mxa}-sgRNA F	CGTTCCACTGAGCGTCAGACGAGGTTCAGGCGAAACCG
oCAH268 P_{mxa}-sgRNA R	GGGATAACGCAGGAAAGAACAAAAAAAGCACCGACTCGGT
oCAH4 pCAH01 F	AAGCTTGACCTGTGAAGTG
oCAH3 pCAH01 R	TTCACTTTTCTCTATCACTGATAG
oCAH952 dCas9 F	gtgatagagaaaagtgaaATGGATAAGAAATACTCAATAGGCTTAGCT
oCAH1507 dCas9 R	cttcacaggtcaagcttTCAGTCACCTCCTAGCTGACTCAAAT
Construction of pJHint and M. capsulatus strain with chromosomal dCas9 integration	
oCAH403 part 1 F	gcagcggaaaagCCCGTAGAAAAGATCAAAGG
oCAH404 part 1 R	cggatcgtgcgcATGTGAGCAAAAGGCCAG
oCAH405 part 2 F	cttttgctcacatGCGCACGATCCGTATTCC
oCAH406 part 2 R	ttaggaattaatcATCTGTCGAAGCGTGCCG
oCAH407 part 3 F	gcttcgacagatGATTAATTCCTAATTTTTGTTGAC
oCAH408 part 3 R	aacgagacatcatACTCTTCCTTTTTCAATATTATTG
oCAH409 part 4 F	aaaaggaagagtATGATGTCTCGTTTAGATAAAAGTAAAGTGATTAACAG
oCAH410 part 4 R	caagggccttgcGCGCGCTCTACGAACTGC
oCAH411 part 5 F	tcgtagagcgcgcGCAAGGCCCTTGGCTCTTG
oCAH412 part 5 R	cttcgcggagctATCTCTCGCAAGACGGCG
oCAH413 part 6 F	tcttgcgagagatAGCTCCGCGAAGTCGCTC
oCAH414 part 6 F	tcttttctacgggCTTTTCCGCTGCATAACCCTG
oCAH447 F	GACGACGACCGTCACAAA
oCAH448 R	GTTTTCGTGATTCGCCGC
Construction of pLSQ and MCA2743(cbbL) PAM mutation	
oCAH1007 pDS1 F	GGATCCAAACTCGAGTAAG
oCAH16 pDS1 R	TAGCCGCTTATGTCTATTGCTG
oCAH1629 P_{cbbL} F	cagcaatagacataagcggctaTTATGCTAATCGCCCTTCATCCG
oCAH1750 *cbbQ* R	gagatccttactcgagtttggatccTCAGAAAAACGTCGCTACGG
oCAH1751 pLSQ F	TGACCGACCTCGACTATTAC
***cbbL*:c.57C>T synthetic fragment**	CGGTAAACCAGCAATAGACATAAGCGGCTATTATGCTAATCGCCCTTCATCCGGCGGTAGCAGGCAGGCATATCAGTATAATGCGCGCTTATTGTCGTGATTATGACAATTTAGTTCCGTTTATGGATATCAGCGCTTATAGTGCCTCGCGAAAAGGGATCGCCCCGATGCCGGCTAGGGAACGGCGGTTCATTGCCATAGCGCTGTTGCAAAACGAGTAGGAGAAAACCATGGCTGTCAAAACATACAACGCGGGCGTCAAGGAATACCGCGAAACCTACTGGGATCCGAACTACACTCCCGCCGACACCGATCTGCTGGCGGTCTTCAAGATCACCCCTCAGCCGGGTGTG

	CCGCGCGAAGAAGCCGCCGCCGCCGTGGCCGCGGAATCG TCGACCGGCACCTGGACCACCGTCTGGACCGACCTGCTG ACCGACCTCGACTATTACAAGGGCCGCG
sgRNA exchange and sgRNA library generation	
oCAH1083 F	taccactccctatcagtgatTGGAACCGTACTGGAACTGC
oCAH1081 R	cttcacaggtcaagcttAAAAAAAGCACCGACTCGGT
oCAH1190 01*sgRNA*^{mrfp} F	GTTTTAGAGCTAGAAATAGCAAGTTAAAATAAGGCT
oCAH119 01*sgRNA* R	ATCACTGATAGGGAGTGGTAAAATAACTCTATCAATGAT AGAG
oCAH1084 *sgRNA*^{cbbL} oligo	TACCACTCCCTATCAGTGATCATTGTCGGCGGGAGTGTAG TTCGTTTTAGAGCTAGAAATAGCAAGTT
oCAH1735 *sgRNA*^{MCA0037} oligo	TACCACTCCCTATCAGTGATTGAGATCGAGGTAAGCGGC GGTTTTAGAGCTAGAAATAGC
oCAH1736 *sgRNA*^{MCA0567} oligo	TACCACTCCCTATCAGTGATCATCTGACGCATGGTAACTG GTTTTAGAGCTAGAAATAGC
oCAH1737 *sgRNA*^{MCA2127} oligo	TACCACTCCCTATCAGTGATGGGCCAGGCGCTCGATCATG GTTTTAGAGCTAGAAATAGC
oCAH1738 *sgRNA*^{MCA2470} oligo	TACCACTCCCTATCAGTGATGCAGTTTTCGGTCACAACAA GTTTTAGAGCTAGAAATAGC
oCAH1739 *sgRNA*^{MCA3033} oligo	TACCACTCCCTATCAGTGATCAGGTGTTGAACTGTTGCGG GTTTTAGAGCTAGAAATAGC
oCAH1018 01sgRNA F	CAACTTGAAAAAGTGGCAC
oCAH1019 01sgRNA R	CTGGGACAGATCATGTCG
oCAH1020 sgRNA^{library} F	gccgacatgatctgtcccagAATCTCCGCCGCTGTTCG
oCAH1021 sgRNA^{library} R	ggtgccactttttcaagttgATAACGGACTAGCCTTATTTTAACTTGC

707 *Lowercase sequence are homology arms for isothermal assembly*

708 **Table 3. Genes with greatest differential sgRNA fitness scores.**

Name	Locus tag	Differential Fitness Score (Log2)	Differential Fitness Score p-value
edd CDS	MCA0037	-3.89	1.6E-71
ispC CDS	MCA0573	-3.59	7.2E-19
sodB CDS	MCA2458	-3.22	2.3E-18
rsxD CDS	MCA2896	-3.21	3.4E-23
dnaA CDS	MCA3033	-3.14	7.0E-22
nitric oxide reductase activation protein NorD CDS	MCA2754	-3.10	2.4E-22
formylmethanofuran dehydrogenase subunit B CDS	MCA2860	-3.08	7.9E-24
rsxG CDS	MCA2897	-3.06	1.1E-49
ferredoxin family protein CDS	MCA2470	-3.02	2.7E-17
frr CDS	MCA0570	-3.01	7.9E-22
rpsB CDS	MCA0567	-2.88	4.8E-22
HAD-IB family hydrolase CDS	MCA2087	-2.87	1.7E-15
rsxA CDS	MCA2893	-2.84	1.7E-19
formylmethanofuran dehydrogenase subunit A CDS	MCA2859	-2.70	6.2E-14
rpsS CDS	MCA2368	-2.68	1.2E-42
cysG CDS	MCA2089	-2.63	2.3E-11
tsf CDS	MCA0568	-2.57	3.9E-14
trxB CDS	MCA1694	-2.56	2.7E-23
pyrH CDS	MCA0569	-2.53	1.8E-13
asnB CDS	MCA2127	-2.43	9.4E-13
infB CDS	MCA1315	-2.36	1.2E-31
sufD CDS	MCA0990	-2.35	5.5E-22
rplD CDS	MCA2371	-2.34	9.5E-21
rplC CDS	MCA2372	-2.28	2.3E-23
CbbQ/NirQ/NorQ/GpvN family protein CDS	MCA2746	-2.24	1.3E-16
OadG family protein CDS	MCA2481	-2.23	2.8E-18
glyQ CDS	MCA2049	-2.22	3.1E-27
ispG CDS	MCA2483	-2.19	9.0E-17
DNA-binding protein CDS	MCA2958	-2.18	1.6E-08
ABC transporter substrate-binding protein CDS	MCA1278	-2.15	9.8E-17
bifunctional cobalt-precorrin-7 (C(5))-methyltransferase/cobalt-precorrin-6B (C(15))-methyltransferase CDS	MCA2296	-2.14	1.0E-12
phosphoribosylaminoimidazolesuccinocarboxamide synthase CDS	MCA0021	-2.08	6.3E-17
calcium/proton transporter CDS	MCA0545	-2.05	1.3E-14
OmpA family protein CDS	MCA1819	1.00	1.5E-08
YihY family inner membrane protein CDS	MCA0711	1.05	1.8E-05
atpA CDS	MCA0010	1.08	8.1E-10
cas5e CDS	MCA0932	1.10	1.2E-07
glutathione S-transferase N-terminal domain-containing protein CDS	MCA1959	1.11	2.9E-07
hypothetical protein CDS	MCA1324	1.14	6.5E-07
phosphoribulokinase CDS	MCA3051	1.15	7.6E-11
NUDIX hydrolase CDS	MCA0333	1.15	7.6E-13
PhoH family protein CDS	MCA1458	1.20	6.2E-07
CbtB-domain containing protein CDS	MCA2302	1.26	6.1E-11
MucB/RseB C-terminal domain-containing protein CDS	MCA1469	1.41	1.2E-08
CbtA family protein CDS	MCA2301	1.61	1.3E-11
RseA family anti-sigma factor CDS	MCA1470	1.62	1.1E-06

709

710 **Supplemental Material**

711

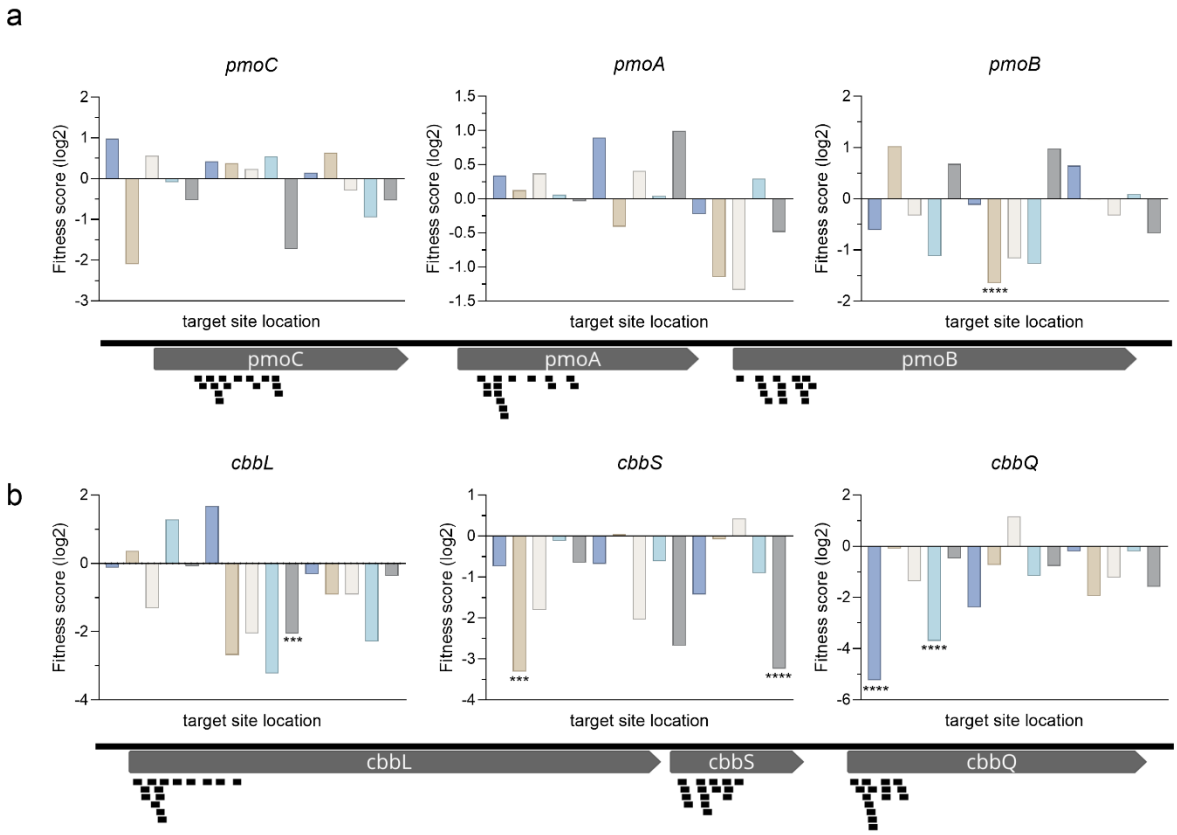

712

713 **Figure S1. Some sgRNAs targeting the same gene have variable differential fitness scores.**
714 a) Mapped sgRNA target sequences (black rectangles) and corresponding differential fitness
715 score within the *M. capsulatus pmoCAB* and *cbbLSQ* operon genes encoding the particulate
716 methane monooxygenase and ribulose-1,5-bisphosphate carboxylase/oxygenase (RubisCO) and
717 associated RubisCO activase, respectively. *** $p \leq 0.001$, **** $p \leq 0.0001$

718

719

720

721

722 Supplemental Tables can be found:
723 https://docs.google.com/spreadsheets/d/1I1Mwm8o_4b5vcYRpeE11nL-bj-
724 knuRPL/edit?usp=drive_link&ouid=103067052205615496775&rtpof=true&sd=true

725